https://doi.org/10.1016/j.apcatb.2019.117824

Highly Efficient Stepwise Electrochemical Degradation of Antibiotics in Water by *in situ* formed $Cu(OH)_2$ Nanowires

Weiran Zheng,[1] *Chui-Shan Tsang,*[2] *Lok Yan So,*[1] *Mengjie Liu,*[1] *Yun-Chung Leung,*[1] *and Lawrence Yoon Suk Lee*[1,]*

[1] Department of Applied Biology and Chemical Technology and the State Key Laboratory of Chemical Biology and Drug Discovery, The Hong Kong Polytechnic University, Hung Hom, Kowloon, Hong Kong SAR, China.

[2] University Research Facility in Life Science, The Hong Kong Polytechnic University, Hung Hom, Kowloon, Hong Kong SAR, China.

*lawrence.ys.lee@polyu.edu.hk (L. Y. S. Lee)

KEYWORDS: $Cu(OH)_2$; ampicillin; tetracycline; chloramphenicol; *in situ* UV-Vis spectroelectrochemistry.

Abstract

The extensive use of antibiotics has been a rapidly growing concern worldwide due to their environmental and health impacts. Electrooxidation is considered a promising route towards antibiotics removal but currently hindered by high overpotential, involvement of noble metals, and strict requirement. We report herein an electrocatalytic system using *in situ* formed $Cu(OH)_2$ nanowires as the electrocatalyst to facilitate the electrooxidation of three common antibiotics (ampicillin, tetracycline, and chloramphenicol). Such $Cu(OH)_2$ nanowires can be formed by Cu(II) species present in wastewater. In our study, the stepwise and potential-dependent electrooxidation process of antibiotics is suggested by voltammetric methods, and low overpotential values (ampicillin: 251 mV, tetracycline: 382 mV, and chloramphenicol: 394 mV) are demonstrated. *In situ* UV-Vis spectroelectrochemical investigations indicate that the $Cu(OH)_y^{x-}$ species on the surface of $Cu(OH)_2$ nanowires acts as the active site *via* the formation of Cu(III)-antibiotics intermediate, which can be regenerated upon the formation and dissociation of Cu(II)-antibiotic complex. Long-term electrooxidation shows the high stability and efficiency of electrochemical removal of antibiotics, and the electron transfer numbers are estimated to be 1.23 (~1) for ampicillin electrooxidation, 4.78 (~5) for tetracycline, and 7.93 (~8) for chloramphenicol at 800 mV (*vs.* Ag/AgCl). UPLC-QTOF-MS results show that the active structural fragments of antibiotics responsible for targeting bacteria are destroyed by electrooxidation and the subsequent activity test using *E. coli* confirms the deactivation of antibiotics. The electrooxidation of all antibiotics shows similar reaction rate with much lower voltage requirements, suggesting its high energy efficiency.

1. Introduction

Antibiotics, one of the most extensively used pharmaceutical materials, have been extensively used and recently emerged as a worldwide concern due to the substantial environmental impact and risks to public health. High concentration of antibiotics, such as ampicillin, tetracycline, and chloramphenicol, has been reported found in the surface and underground water globally as a result of urban wastewater discharge [1-3], which can lead to severe consequences, especially antibiotic resistance of bacteria [3]. The current method of removing antibiotics from wastewater includes adsorption [4], membrane separation [5], biological approach [6], advanced oxidation processes (AOPs) [7], and photocatalysis [8]. These methods, however, have one or more drawbacks of inefficiency, secondary contamination, and/or the complication of post-treatment, and thus a more precise and simple way of antibiotics removal is in demand.

Most antibiotics contain electron-donor groups that are designed to target specific binding sites of bacteria during the pharmacokinetic process, making them suitable for electrochemical oxidation [9]. During the past decade, electrochemical methods have attracted particular research interests as a promising approach for the removal and degradation of antibiotics at low cost. Notably, the Electro-Fenton (EF) process, the cathodic electro-generation of H_2O_2 in the presence of dissolved O_2, has been proved to be both simple and highly efficient for decontamination of wastewater with organic pollutants [10, 11]. The production of hydroxyl radical (redox potential = 2.72 V *vs.* NHE) on metal oxide-based electrodes, such as Ti/RuO_2 [12], Fe_3O_4 [13], MnO_x [14], and IrO_2 [15], is essential for the degradation process. However, such EF process has shortcomings, such as the needs for continuous O_2 supply, high voltage bias, and sometimes the involvement of noble metal [10]. Therefore, direct electrooxidation of antibiotics at low voltage without O_2 demand is highly desired, and a few catalysts have been developed. For example, ofloxacin can be

oxidized on a Ti/Pt electrode [16] and flutriafol can be degraded using PbO_2 [17], however, high overpotentials are often required (>1.2 V). With the rapid development in electrocatalytic materials driven by energy-related researches, more candidates are yet to be explored for antibiotics electrooxidation.

It is desirable to identify other catalytic species that can reduce the high overpotential required for the hydroxyl radical production. Cu species with its unique Cu(II)-Cu(III) redox couple [18, 19] has been intensively studied in electrochemistry due to its versatile applications such as glucose sensing [20]. Cu species are also commonly found in wastewater (up to 30 μM [21]). It would be ideal to engage these Cu ions in wastewater as the electrocatalyst for antibiotic electrooxidation, which can reduce the use of other heavy metals-based catalysts and thus the secondary contamination. However, the electrooxidation of antibiotics using $Cu(OH)_2$ has not been studied yet.

In this work, the electrooxidation of three antibiotics (ampicillin, tetracycline, and chloramphenicol) commonly found in wastewater are investigated using *in situ* formed $Cu(OH)_2$ as an electrocatalyst. The morphology and structure of the $Cu(OH)_2$ are examined, followed by the spectroscopic investigation of Cu(II)-antibiotic interaction. The mechanism of electrochemical polarization process, as well as the long-term stability and electrooxidation route of all three antibiotics, are assessed in detail *via* voltammetric and *in situ* UV-Vis spectroelectrochemical methods. The electrolysis products at different voltage bias are analyzed using ultra-performance liquid chromatography-mass spectrometer (UPLC-MS), and the potential-dependent reaction mechanisms of all three antibiotics are proposed. Finally, the antibiotic activities before and after the electrooxidation treatment are further checked against *Escherichia coli*, confirming their successful degradation.

2. Experimental

2.1 Chemicals

Sodium hydroxide (>96%, UNI-CHEM), ampicillin sodium salt (Sigma-Aldrich), tetracycline (Sigma-Aldrich), chloramphenicol (≥98%, Sigma-Aldrich), and copper(II) nitrate (Sigma-Aldrich) were used as received. All aqueous solutions were prepared using doubly deionized water (DI water) from MilliQ Water System (Millipore, USA, R>18.2 MΩ cm^{-1}).

2.2 Material characterization and analysis

Transmission electron microscopic (TEM) images were obtained using a TEM instrument from JEOL (Model JEM-2100F) equipped with an energy-dispersive X-ray spectrometer (EDS) for the elemental distribution mapping of material. The X-ray powder diffraction (XRD) patterns were measured on a SmartLab X-ray diffractometer (Rigaku, voltage 45 kV, current 200 mA) to analyze the crystal structure of the material. The XRD simulation was obtained by CrystalDiffract using $Cu(OH)_2$ model structure with 5 nm diameter. X-ray photoelectron spectroscopy (XPS) spectra were acquired using a Thermo Fisher ESCALAB 250Xi. The C 1s peak at 284.6 eV is used for calibration.

The electrooxidation products were analyzed using a UPLC-MS. The analyses were performed on an Agilent 6540 liquid chromatography-electrospray ionization quadrupole-time-of-flight mass spectrometer (UPLC-QTOF-MS). Liquid chromatographic separation was performed on a Zorbax C18 column (2.1 × 50 mm, 1.8 μm, Agilent), and preceded by a C18 guard column (2.1 × 5 mm, 1.8 μm, Agilent), with a column temperature of 25 °C. A mixture of water (solvent A) and acetonitrile with 0.1 % formic acid (solvent B) was used as a mobile phase at a flow rate of 0.3 mL/min. At the beginning of the analysis, the analyte was eluted with a solvent mixture of 2% solvent B, followed by 80 % solvent B over 12 min, and then back to 2% solvent B over 0.5

min. The total analysis time was 15 min, and the injection volume was 2 μL. The analytes were ionized with an electrospray ionization (ESI) source in positive mode under the following condition: ion spray voltage 4,500 V, gas temperature 300 °C, nebulizer pressure 35 psi, sheath gas temperature 270 °C, nozzle voltage 1,000 V, fragmentor voltage 175 kV, and skimmer voltage 65 V. The other parameters were fixed for the tuning file. The mass spectra were recorded in the range m/z 100–1,700.

2.3 Electrochemical tests

A three-electrode system was adopted for cyclic voltammetric (CV) electrochemical analysis with glassy carbon electrode (GCE, 3 mm diameter, surface area = 0.07 cm^2) as working electrode, saturated calomel electrode (SCE) as the reference electrode, and Pt wire as the counter electrode in 0.1 M NaOH electrolyte (pH = 13.07) using a CHI 760E electrochemical analyzer (CH Instruments, Inc., USA). For direct current (dc) voltammetry, the scan rate was 5 mV s^{-1}. For Fourier transformed alternating current voltammetry (FTacV) tests, the frequency was 9 Hz and an amplitude of 80 mV was applied.

To perform the electrocatalysis, the copper(II) nitrate aqueous solution was added to 0.1 M NaOH with continuous stirring to form light-blue $Cu(OH)_2$ colloid solution with various concentrations. The antibiotic aqueous solution was then introduced to the colloid solution to reach an equilibrium, and the mixed solution was engaged as the electrolyte.

For *in situ* UV-visible (UV-Vis) spectroelectrochemical studies, an integrated spectroelectrochemical system (Pine Research Instrumentation, Inc., USA) was employed including an AvaLight UV/Vis/NIR light source, an AvaSpex-UL S2048 Fiber-Optic spectrometer, and a WaveDriver 20 benchtop potentiostat/galvanostat System. The spectroelectrochemical cell consists of a gold honeycomb electrode (integrated with both working and counter electrode), a

low-profile silver chloride (Ag/AgCl/KCl 3.0 M) reference electrode, and a standard quartz cuvette. A staircase cyclic voltammetric (SCV) method was used for the UV-Vis spectroelectrochemical study with an amplitude of 5 mV and a period of 10 s. For long-term electrolysis coupled with *in situ* UV-Vis spectroscopy, each UV-Vis spectrum was collected every 15 s. The working electrode is GCE, and the electrolyte volume is 2.5 mL for all spectroelectrochemical studies. The spectral data were analyzed by SpectraGryph software.

For potential-dependent electrooxidation of antibiotics, two potentials, 500 and 800 mV (*vs.* SCE) were applied, and the working electrode is GCE. The total electrolysis time is 4 hours.

2.4 Antibacterial activity evaluation

The antibacterial activity is evaluated by the minimum inhibitory concentration (MIC), which is the lowest concentration of a chemical which inhibits the visible growth of a bacterium. MICs of three antibiotics including ampicillin, tetracycline, and chloramphenicol against *Escherichia coli* (*E. Coli*) K-12 were determined using the reported method [22]. Briefly, the experiment was performed in a 96-well plate with the serial two-fold dilution of antibiotics (before and after electrooxidation, pH = 7.0) across the columns from left to right. The maximum tested concentration of each antibiotic was 50 μM. Each dilution was performed in duplicate. Each well contains 80 μL of the medium, 10 μL of antibiotics, and 10 μL of bacterial culture (to give a final CFU/mL of *ca.* 5×10^6). Controls with bacterium and medium only were included in the last two columns, respectively, to ensure the viability of bacterium and the sterility of the medium. The plates were then incubated at 37 °C for 18 hours before recording the results.

3. Results and discussion

3.1 *In situ* formation of $Cu(OH)_2$ nanowires and characterization

The formation of light-blue $Cu(OH)_2$ colloid in NaOH solution is observed immediately after adding Cu(II) salt solution to NaOH electrolyte. At pH = 13.07, the majority (> 98%) of Cu(II) ions exists as $Cu(OH)_2$(s) in 0.1 M NaOH aqueous solution, with the trace amounts of $Cu(OH)_3^-$ and $Cu(OH)_4^{2-}$ [23] (**Equation 1, Figure S1**). No significant pH change is observed after adding 1 mM Cu(II) (maintaining at 13.07).

$$Cu(II) + 2OH^- \rightarrow Cu(OH)_2 \qquad \text{(Equation 1)}$$

Figure 1a shows a typical TEM image of the congregated nanowire structures formed in 0.1 M NaOH solution containing 1 mM Cu(II) ion (denoted as 1 mM $Cu(OH)_2$). The selected area electron diffraction (SAED) pattern shown in **Figure 1b** indicates the formation of a polycrystalline structure and can be indexed as the (110), (111), (130), (132), and (200) rings of the orthorhombic $Cu(OH)_2$ structure [24]. The dark-field TEM image in **Figure 1c** and its corresponding Cu elemental mapping in **Figure 1d** confirms the presence of $Cu(OH)_2$ in the form of nanowires. A closer observation of a single nanowire, as shown by the high-resolution TEM (HRTEM) in **Figure 1e**, acknowledges the polycrystalline structure. The interplanar spacing (*d* spacing) of *ca.* 0.289 nm measured at the center of the nanowire matches well with that of (110) planes of $Cu(OH)_2$, while the values of *ca.* 0.259 and 0.240 nm are assigned to the (002) and (022) planes, respectively [24]. The distinctive orthorhombic $Cu(OH)_2$ structure is also suggested by the experimental XRD pattern (**Figure 1f**), which can be assigned exclusively to $Cu(OH)_2$ (JCPDS 35-0505) and matches well with the simulation results for $Cu(OH)_2$. The broad peaks indicate the poor crystallinity of formed $Cu(OH)_2$ nanowires with a crystallite size of 4.71 nm, estimated by the Scherrer equation using (021) peak. Such a small nanocrystal size agrees with the HRTEM image, showing the formation of nanowires *via* the assemble of $Cu(OH)_2$ nanocrystals. Notably, the relative intensity ratio of (020) to (021) planes is higher than the previous report [25], implying

the selective exposure of (020) plane. To clarify, the structure of $Cu(OH)_2$ [26] is illustrated in **Figure 1g**, as well as its dominating (020), (021), and (002) planes. The layered structure of $Cu(OH)_2$ formed *via* Cu-O bonding features one-dimensional growth, and both (020) and (021) planes as the primary interfaces between $Cu(OH)_2$ and environments can provide direct access to the Cu atoms. The surface species status of the $Cu(OH)_2$ nanowire is studied by XPS. **Figure 1h** shows the survey spectrum and the peak fitting results of the O 1s spectrum. As expected, both Cu and O are evident on the surface, and the atomic ratio between O and Cu is 2.20, slightly higher than the stoichiometric ratio of 2. It can be attributed to the physisorbed H_2O and/or the exposure of (020) plane (terminated by O atoms). The existence of physisorbed H_2O is revealed by the O 1s peak at 532.3 eV, well distinguished from the O species from $Cu(OH)_2$ at 530.9 eV.

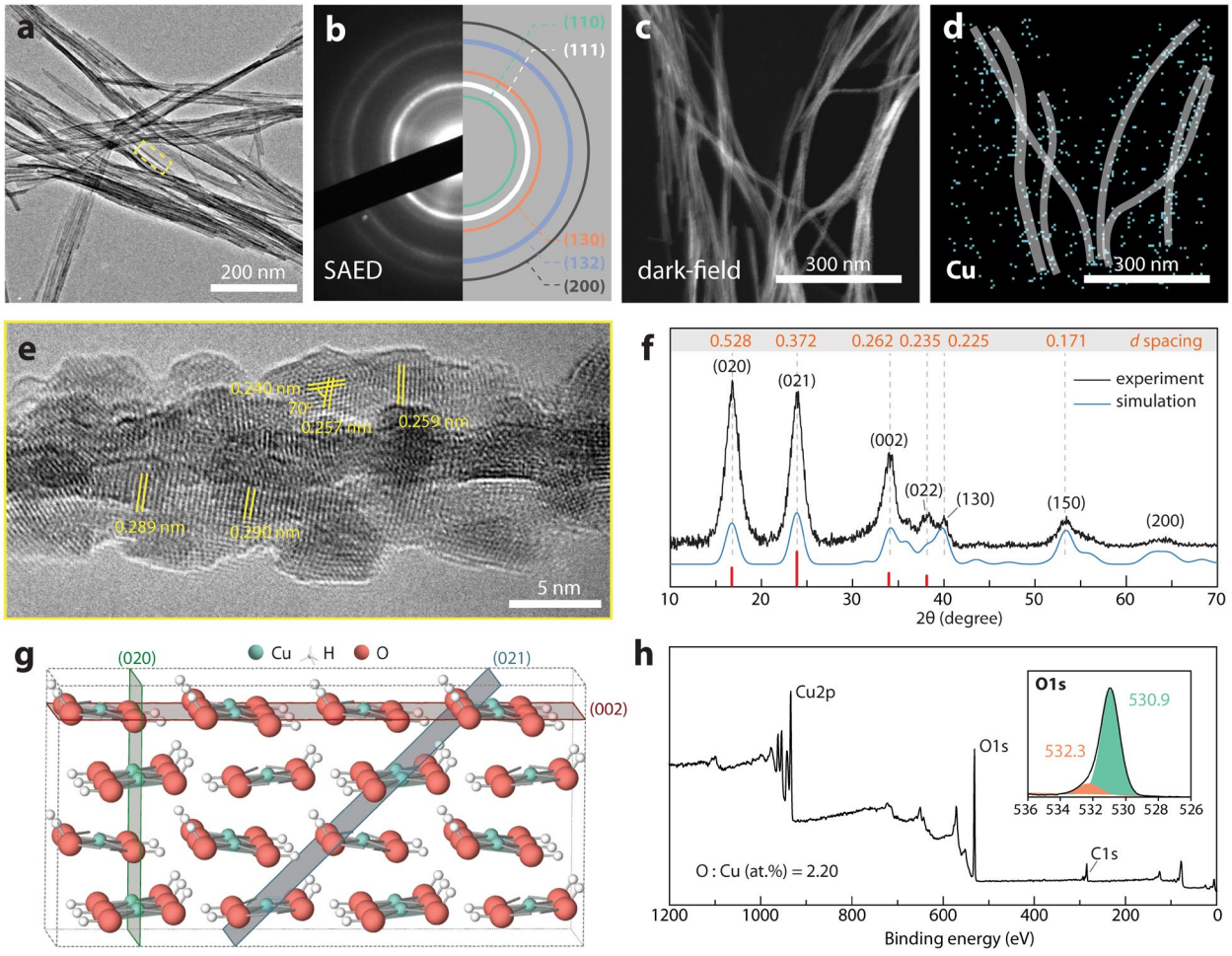

Figure 1. (a) TEM image of *in situ* formed $Cu(OH)_2$ nanowires; (b) SAED pattern of aggregated nanowires; (c) Dark-field TEM image of nanowires; (d) Elemental mapping of Cu of the dark-field image. The nanowires are outlined to help visualization; (e) HRTEM image of the selected region in nanowire (a); (f) Experimental and simulated XRD patterns of *in situ* formed $Cu(OH)_2$ nanowires. The corresponding *d* spacing values of planes are given at the top; (g) Structural illustration of $Cu(OH)_2$ showing the (020), (021), and (002) planes; (h) XPS survey spectrum of *in situ* formed $Cu(OH)_2$ nanowires. Inset is the fitted O1s region.

3.2 Antibiotic-$Cu(OH)_2$ interaction

The study of the interaction between antibiotics and $Cu(OH)_2$ species is essential for further electrochemical analysis. The formation of Cu(II)-antibiotic complex (**Equation 2**) has been widely reported in the literature [27-29], and the most preferred configurations of studied antibiotics are shown in **Figures 2a-2c**. The structural fragments of the antibiotics marked in green are generally considered to be responsible for targeting cell wall synthesis, protein synthesis, nucleic acids, metabolic pathways, and membrane of bacteria [9]. Thus, the successful degradation of antibiotics requires the destruction of these fragments.

$$\text{Cu(II)} + \text{antibiotic} \leftrightarrow \text{Cu(II)-antibiotic complex} \qquad \text{(Equation 2)}$$

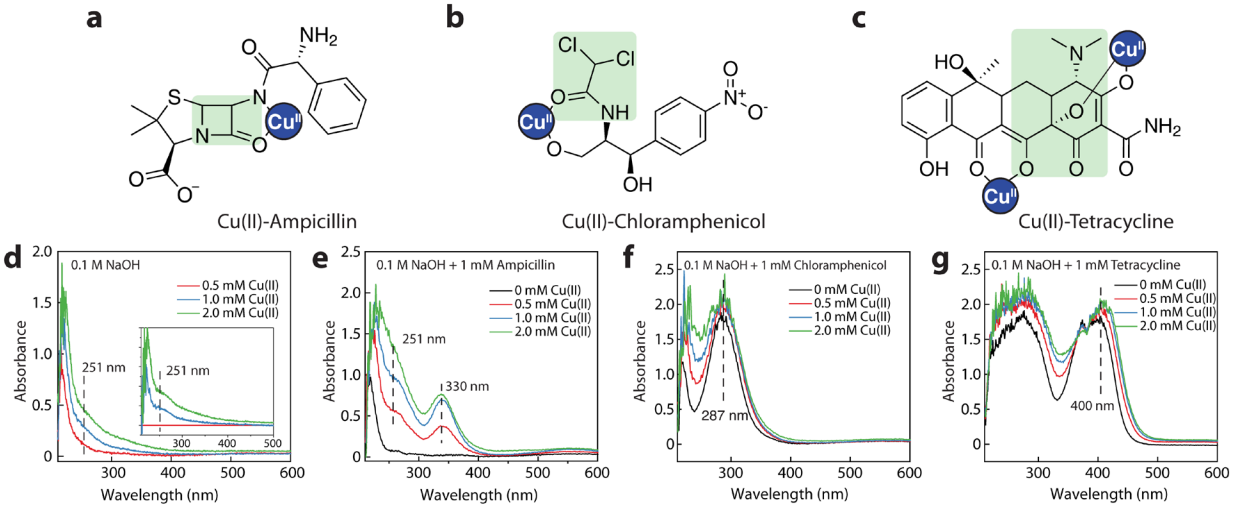

Figure 2. (a-c) Proposed antibiotic-Cu(II) coordination structures based on literature reports: (a) ampicillin; (b) chloramphenicol; (c) tetracycline. (d) UV-Vis absorbance spectra of 0.1 M NaOH solution containing different

concentration of Cu(II) ion (0.5, 1.0, and 2.0 mM). Inset shows the subtracted spectra using 0.5 mM Cu(II) one as reference spectrum; (e-g) UV-Vis absorbance spectra of (e) ampicillin, (f) chloramphenicol, and (g) tetracycline in 0.1 M NaOH solution with different concentration of Cu(II) ion (0, 0.5, 1.0, and 2.0 mM).

The interaction between Cu(II) and antibiotics is studied using UV-Vis spectroscopy. As shown in **Figure 2d**, $Cu(OH)_2$ suspension (0.5 mM) has an absorption edge at around 251 nm. The further increment of Cu(II) ion concentration to 2.0 mM leads to the shift of absorption edge towards ~330 nm. The differential spectra in the inset indicate the evolution of a peak at 251 nm and a broad absorption band at approximately 300 nm, which can be attributed to the formed soluble cuprous ions, such as $Cu(OH)_3^-$ and $Cu(OH)_4^{2-}$, and $Cu(OH)_2$ [30]. It is well known that the shape and size of nanomaterials affect its band structure. The shift of the absorption edge is attributed to the increased $Cu(OH)_2$ particle size, and the broad absorption band may be due to the surface defects on the *in situ* formed $Cu(OH)_2$ nanowires which give rise to the intragap states [31].

The UV-Vis spectra in the presence of 1 mM antibiotics and different concentration of $Cu(OH)_2$ are shown in **Figures 2e** (ampicillin), **2f** (chloramphenicol), and **2g** (tetracycline). Ampicillin solution shows only one absorption band below 240 nm, while two new absorption bands are observed (~251 and 330 nm) after the addition of Cu(II). Such spectroscopic changes are associated with the dramatic solution color change from colorless to violet, due to the formation of Cu(II)-ampicillin complex *via* the β-lactam groups (-CO-NH-, **Figure 2a**) [32]. The peak intensity at 330 nm doubles as Cu(II) concentration increases from 0.5 to 1.0 mM, while only minor enhancement is obtained from 1.0 to 2.0 mM, suggesting a stable 1:1 coordination between Cu(II) sites and ampicillin. Different from ampicillin, both chloramphenicol and tetracycline show their distinctive UV-Vis spectra in alkaline solution with the characteristic absorption bands at 287 and 400 nm, respectively. The introduction of $Cu(OH)_2$ to both chloramphenicol and tetracycline solutions shows an inapparent impact on the spectrum with slightly red-shifted band edge and

enhanced absorbance (**Figures 2e** and **2f**). Such results suggest a weak interaction between chloramphenicol/tetracycline and $Cu(OH)_2$, as previously reported for both chloramphenicol [27] and tetracycline [33].

3.3 Antibiotics electrochemistry on $Cu(OH)_2$: voltammetry study

The electrochemical behavior of antibiotics with *in situ* formed $Cu(OH)_2$ is studied using CV (both dc voltammetry and FTacV) with a bare GCE as the working electrode in 0.1 M NaOH electrolyte containing 1 mM $Cu(OH)_2$ and various concentrations of antibiotics. The results are plotted in **Figure 3** (**a** and **d**: ampicillin; **b** and **e**: tetracycline; **c** and **f**: chloramphenicol), and the CV curves measured with/without Cu^{2+} species in the absence of antibiotics are provided for comparison.

For dc voltammetry, the current signal originates from both non-Faradic and Faradic process. The former one is mainly the formation of adsorption layers on the surface of electrode materials or the establishment of the electrochemical double layer (EDL). The current signal obtained sweeping GCE in 0.1 M NaOH from 0 to 0.8 V is the typical non-Faradic current. (curve i in **Figure 3**) The Faradic current, or electrocatalytic current, is related to the electron transfer process between substance and the electrode.

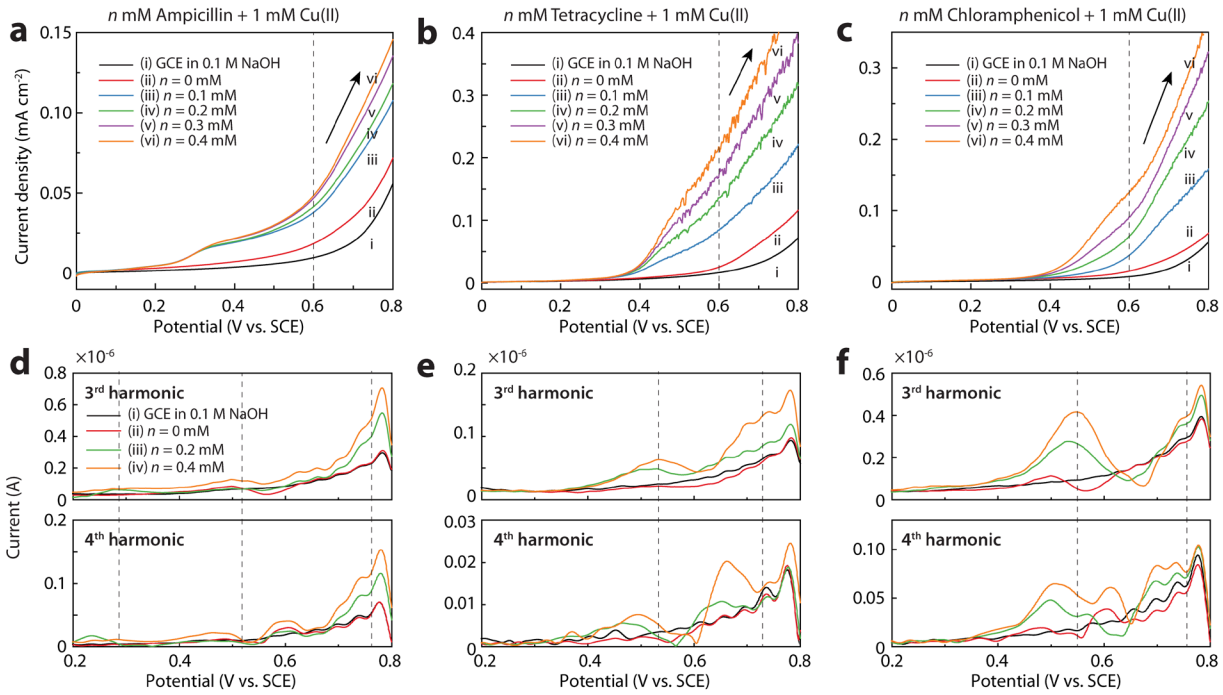

Figure 3. dc voltammograms (a-c) and FTacV plots (d-f) of various concentrations (dc: 0.1, 0.2, 0.3, and 0.4 mM; ac: 0.2 and 0.4 mM) of (a, d) ampicillin, (b, e) tetracycline, and (c, f) chloramphenicol in 0.1 M NaOH aqueous solution with *in situ* formed $Cu(OH)_2$ as electrocatalyst (total Cu(II) concentration is 1 mM). For FTacV, the third and fourth harmonic components are presented. Only forward scans are shown for clarity.

In our study, with 1 mM $Cu(OH)_2$ present, a universal increment of current density was observed from ~400 mV (*vs.* SCE, if not stated otherwise, **Figures 2a-2c**), which can be assigned to the electrooxidation of Cu(II) to Cu(III) (**Equation 2**) [19, 34]. Upon the addition of antibiotics, the current dramatically rises (mostly Faradic current), which indicates the electrooxidation of antibiotics. A further increment of antibiotics concentration (from 0.1 to 0.4 mM) results in a higher oxidation current, as expected. It is worth to note that the onset potential read from dc voltammograms depends on the type of antibiotics. For ampicillin, the oxidation signal starts from ~250 mV, lower than that of tetracycline (~382 mV), and chloramphenicol (~394 mV). Such differences could be the combined results of both antibiotic structures and reaction mechanism.

$$Cu(OH)_2 + OH^- \rightarrow CuOOH + H_2O + e^- \qquad \text{(Equation 3)}$$

Unlike dc voltammetry, FTacV, developed by the Monash Electrochemistry Group, can provide insights towards the electrochemical processes and distinguish the non-Faradic and Faradic signals [35]. In principle, the non-Faradic current is only present in the dc and fundamental harmonic components, while higher harmonic components reveal only the faster electron transfer kinetics between the electrode and the pre-adsorbed substance (Cu(II)-antibiotics complex in our case). Thus, it is possible to analyze the exact potential for electron transfer and estimate the relative rate using the 3rd and 4th harmonic components of FTacV, as given in **Figures 3d-3f**. The valley potentials of the 4th harmonic components and peak potentials of the 3rd indicate the formal reversible potential of Cu(II)-antibiotics complex. In the absence of antibiotics, the 3rd and 4th harmonic components show an insignificant difference in the electrolyte regardless of the presence of $Cu(OH)_2$. The slight current enhancement at ~570 mV suggests a rather slow Cu(II) to Cu(III) electrooxidation. After adding antibiotics, a current boost is evident for all antibiotics, and further increment of antibiotics concentration results in a higher current signal, a clear indication that the electrocatalytic process involves fast electron transfer. Specifically, for ampicillin, three electron transfer processes are evident at 284, 520, and 765 mV, with increasing electron transfer rate (increasing current peak intensity). The first process located at 284 mV is probably not related to the Cu(II) to Cu(III) electrooxidation but the Cu(I) to Cu(II) process. The Cu(I) is the chemical reduction product of surface Cu(II) species on $Cu(OH)_2$ by the adsorbed reductive ampicillin. The second process at 520 mV indicates the Cu(II) to Cu(III) electrooxidation, and the last one at 765 mV suggests the fastest electron transfer, presumably the catalytic oxidation of ampicillin. For tetracycline, two processes are suggested at 535 and 718 mV, which can be attributed to Cu(II) to Cu(III) and tetracycline oxidation, respectively. As to chloramphenicol, a massive peak at 550 mV shows a fast Cu(II) to Cu(III) electrooxidation, and the smaller current increment (compared to the

current obtained without chloramphenicol) at 758 mV implies a slower electrooxidation process. However, it should be noted that the FTacV results provide the information only on electron transfer processes, yet the combination of electron transfer processes and their coupled chemical reactions are unknown. Also, due to the most likely multistep electrooxidation of antibiotics, their reaction intermediates and the changes of complex configurations (redox reaction between Cu(II) and antibiotics) cannot be obtained by voltammetric methods.

3.4 Kinetic aspects of antibiotics electrooxidation

The kinetic aspects of electrooxidation process are discussed based on the dc voltammetric investigations. **Figure 4a** displays the linear correlation between the antibiotics concentration and the current density at 600 mV (from CV data of **Figures 3a-3c**), with the fitted slope values. The linear relationship found in all cases indicates that the electrooxidation of antibiotics is controlled by the electron transfer between electrode and antibiotics molecules within the studied concentration range between 0.1 and 0.4 mM, rather than the mass transfer of antibiotics. If the *in situ* formed $Cu(OH)_2$ nanowires are considered as an antibiotic electrochemical sensor, the slope value can be used to estimate the sensitivity at 600 mV: 45.1 mA mM^{-1} cm^{-2} for ampicillin, 271.6 mA mM^{-1} cm^{-2} for chloramphenicol, and 443.5 mA mM^{-1} cm^{-2} for tetracycline, which are significantly higher than previous reports on ampicillin [36], chloramphenicol [37, 38], and tetracycline [39, 40].

To better understand the electrooxidation process, the Tafel plots are constructed based on the corresponding CVs (**Figure 4b**). Within the studied oxidation range (300 to 800 mV), the electrooxidation of Cu(II) to Cu(III) species shows a linear correlation with a Tafel slope of 374 mV dec^{-1}, suggesting only one primary electron transfer reaction occurs in the process. In the presence of chloramphenicol, the Tafel curve remains linear with a slope of 249 mV dec^{-1},

suggesting that the electrooxidation of chloramphenicol is kinetically favored than the Cu(II) electrooxidation. For ampicillin and tetracycline cases, two distinct linear regions are observed, which can be attributed to the stepwise electrooxidation of different functional groups in the antibiotic molecule. These results are in good agreement with the reported stepwise electrooxidation of tetracycline on Pt nanoparticles [40].

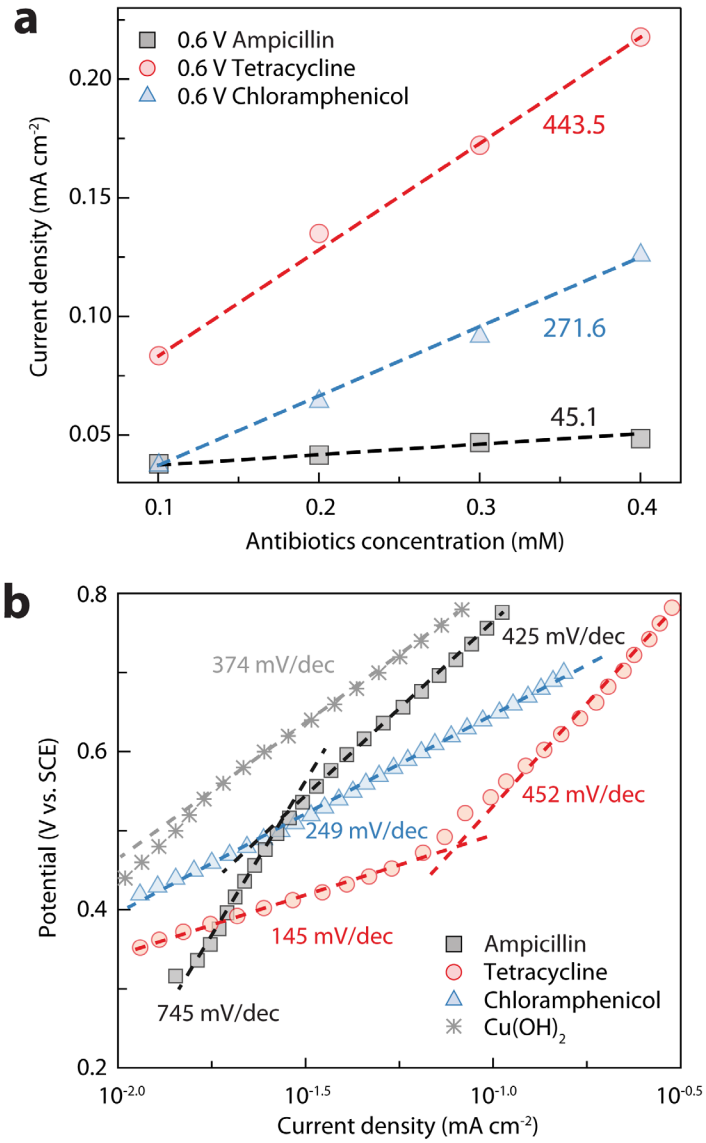

Figure 4. (a) Relationship between current density at 600 mV (*vs.* SCE) and antibiotics concentration. The inserted values are the slope of the correlation curve; (b) Tafel plots of $Cu(OH)_2$ and antibiotics electrooxidation calculated from the corresponding CV (antibiotics: 0.2 mM). The inserted values are the Tafel slope.

The charge transfer coefficient, another key kinetic parameter for catalysis evaluation, is calculated based on the Tafel slope measured, following $\alpha = \frac{RT}{F} \cdot \frac{1}{dE/dlni} = \frac{2.3RT}{F} \cdot \frac{1}{dE/dlogi}$ for a multistep electrochemical process removing the factor *n* (see the **Figures S2-S5**, Supporting Information) [41]. **Table 1** summarizes the key aspects of the electrooxidation of both *in situ* formed $Cu(OH)_2$ and antibiotics in 0.1 M NaOH electrolyte.

Table 1. The key kinetic aspects of the electrooxidation of both *in situ* formed $Cu(OH)_2$ and antibiotics.

	$Cu(OH)_2$	**ampicillin**	**tetracycline**	**chloramphenicol**
Tafel slope[1] ($mV\ dec^{-1}$)	374 (0.50~0.80 V)	745 (0.30~0.50 V) 425 (0.50~0.80 V)	145 (0.35 ~ 0.45 V) 452 (0.45~0.80 V)	249 (0.30~0.80 V)
Charge transfer coefficient[2] α	0.160 (0.50~0.80 V)	0.0739 (0.30~0.50 V) 0.138 (0.50~0.80 V)	0.409 (0.35 ~ 0.45 V) 0.130 (0.45~0.80 V)	0.235 (0.30~0.80 V)
Electron transfer number[3]	n/a	1.23	4.78	7.93
Kinetic constant[4] (min^{-1}) × 10^{-3}	n/a	68.1	35.4	11.5

[1] Tafel slopes are obtained from the CVs measured at 5 mV s^{-1} with antibiotics concentration of 0.2 mM.

[2] The charge transfer coefficients are calculated from total current, not current density. The electron transfer number is ignored due to a multi-product and multi-step electrooxidation process of antibiotics.[41]

[3] The electron transfer number is calculated based on *in situ* spectroelectrochemical measurements at 800 mV (*vs.* Ag/AgCl).

[4] The kinetic constant (*k*) is calculated assuming a first-order kinetic applies: $\ln\frac{C}{C_0} = -kt$, where C_0 is the initial concentration of antibiotics and C is the concentration at time = t. The concentration of antibiotics is calculated based on *in situ* spectroelectrochemical measurement at 800 mV with 10 mM antibiotics and 0.1 mM $Cu(OH)_2$.

3.5 *In situ* UV-Vis spectroelectrochemical study

The *in situ* UV-Vis spectroelectrochemical method is employed to study the reaction mechanism of antibiotic electrooxidation using *in situ* formed $Cu(OH)_2$ nanowires as an electrocatalyst. **Figure 5a** illustrates the setup of the cell for spectroelectrochemistry, and **Figure S6** shows the digital images of the experimental setup. An integrated Au honeycomb electrode was used as both working and counter electrodes (the front view is shown in **Figure 5b**), and an

Ag/AgCl/KCl (3.0 M) electrode was employed as a reference electrode. During the electrochemical process, the reaction was confined within the honeycomb area/tunnels where the UV-Vis light could pass.

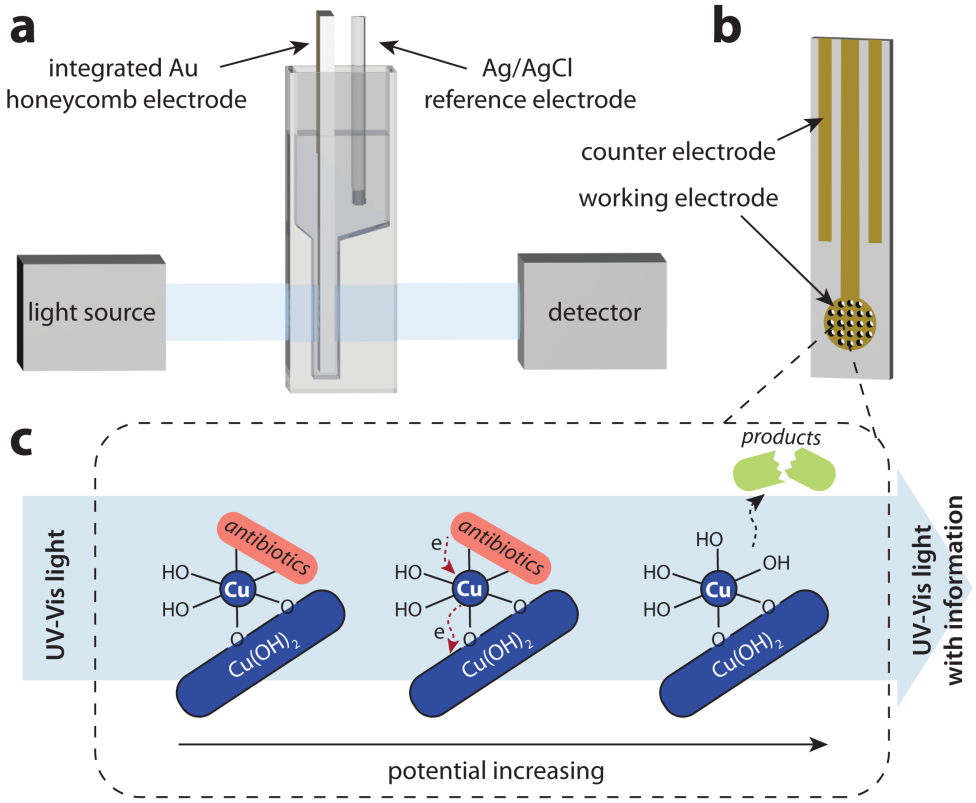

Figure 5. (a) Illustration of *in situ* UV-Vis spectroelectrochemical cell setup. The side view of the cell is shown here; (b) Front view of the gold honeycomb electrode; (c) A simplified illustration of electrooxidation of antibiotic molecules by $Cu(OH)_2$ in the *in situ* experiments.

Figure 5c shows a simplified illustration of the electrooxidation of antibiotics. Inside the tunnels of honeycomb working electrode, the antibiotics are coordinated with $Cu(OH)_2$ species. For ampicillin, the strong interaction with Cu (II) is likely to result in a homogeneous Cu(II)-ampicillin complex with low content of remaining $Cu(OH)_2$ structure. However, both chloramphenicol and tetracycline weakly interact with Cu(II), thus only be absorbed on the surface

of $Cu(OH)_2$ nanowires. With increasing potential, either Cu(II)-antibiotic complex or surface Cu(II) species loses electrons to the electrode, eventually results in the oxidation of antibiotic molecules. The oxidation products then can be released into the electrolyte while the surface Cu sites are renewed.

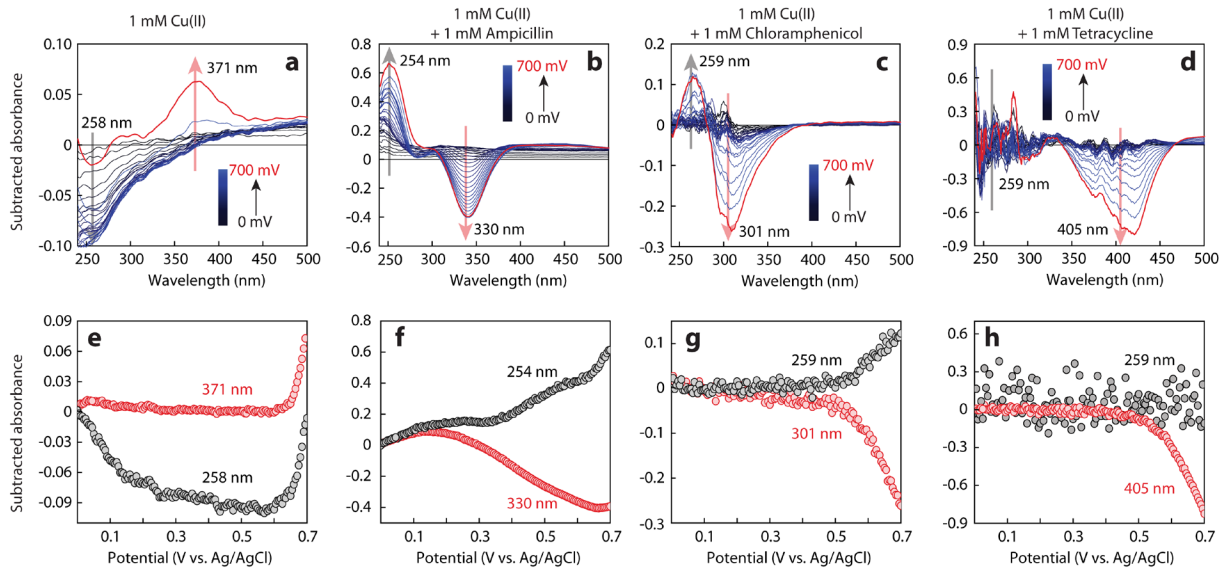

Figure 6. (a-d) Evolution of the differential *in situ* UV-Vis absorbance spectra with potential: (a) $Cu(OH)_2$, (b) $Cu(OH)_2$ with 1 mM ampicillin, (c) $Cu(OH)_2$ with 1 mM chloramphenicol, and (d) $Cu(OH)_2$ with 1 mM tetracycline. The potential interval is 20 mV, and the last spectrum at 700 mV is highlighted in red. The spectrum at 0 V (*vs.* Ag/AgCl) is used as background, and only positive scans are shown for clarity; (e-h) Correlation between potential and absorbance of selected peak position: (e) $Cu(OH)_2$ (371 and 258 nm), (f) $Cu(OH)_2$ with 1 mM ampicillin (330 and 254 nm), (g) $Cu(OH)_2$ with 1 mM chloramphenicol (301 and 259 nm), and (h) $Cu(OH)_2$ with 1 mM tetracycline (405 and 259 nm).

Figure 6 shows the *in situ* UV-Vis spectroelectrochemical results. The staircase cyclic voltammetry (SCV) of the corresponding spectroelectrochemical studies are shown in **Figure S7**. **Figures 6a-6d** present the corresponding *in situ* UV-Vis spectra of each SCV process. The spectrum at 0 V (*vs.* Ag/AgCl) was used as background, and only those associated with positive scan were plotted for clarity. **Figures 6e-6h** show the correlation between the absorbance of the

selected band and the applied potential. For $Cu(OH)_2$ electrooxidation, the intensity of two bands at 258 and 371 nm show a significant dependence on the potential. The band at 258 nm decreases as the potential changes from 0 to 350 mV (*vs.* Ag/AgCl, **Figure 6e**), which can be attributed to the transition of soluble cuprous ions to $Cu(OH)_2$ on the surface of nanowires [42]. At the potential higher than 600 mV (*vs.* Ag/AgCl), the intensities of both bands rapidly grow, due to the formation of CuO nanostructure that has strong absorption bands at 260 and 370 nm [43]. For ampicillin electrooxidation, two bands at 254 and 330 nm also show the potential-related intensity changes (**Figure 6b**). From ~200 mV (*vs.* Ag/AgCl), the intensity of the band (λ = 330 nm) due to Cu(II)-ampicillin complex declines monotonically, showing a steady consumption of the complex. In contrast, the band at 254 nm increases with the consumption of ampicillin. Considering the 1:1 coordination between Cu(II) and ampicillin, this band is assigned to the released soluble Cu(II) species. For chloramphenicol, two major absorption bands at 259 and 301 nm exhibit the intensity changes upon the potential scan (**Figure 6c**), which are attributed to the soluble Cu(II) sites ($Cu(OH)_x^{y-}$ on $Cu(OH)_2$ surface) and chloramphenicol, respectively. At the applied potentials higher than 500 mV (*vs.* Ag/AgCl), both the consumption of chloramphenicol and the release of soluble Cu(II) species are evident (**Figure 6g**). From the tetracycline electrooxidation, a broad absorption band (350 to 450 nm) is observed to change the intensity, which is related to the consumption of tetracycline (**Figure 6d**). However, the band at 259 nm is rather noisy and remains within a similar intensity range over the potential scan (**Figure 6h**). It is possible that the renewed Cu(II) sites are still somehow coordinated with the oxidation products.

The similar trend found from *in situ* spectroelectrochemical results of three antibiotics indicates that the Cu(II)-antibiotic interaction is essential for antibiotic electrooxidation. It is interesting that, for ampicillin, the concentration starts to decrease from 200 mV (*vs.* Ag/AgCl), a

significantly lower potential than that of Cu(II) and the other two antibiotics. Based on the FTacV results (**Figure 3a**), the oxidation of ampicillin involves a slow oxidation process at ~284 mV, which is possibly related to the Cu(I) to Cu(II) electrooxidation where the Cu(I) species originates from intra-molecular redox between ampicillin and Cu(II). For chloramphenicol and tetracycline, the significant drop of their concentration occurs at a potential higher than 550 mV (*vs.* Ag/AgCl). This suggests that a Cu(II) to Cu(III) oxidation is essential for the electrooxidation of both, similar to the previous report on glucose electrooxidation on Cu based materials [44].

3.6 Long-term electrooxidation of antibiotics monitored by *in situ* UV-Vis spectroscopy

Long-term electrooxidation of antibiotics coupled with *in situ* UV-Vis spectroscopy is engaged to evaluate the efficiency of electrochemical degradation of antibiotics in water. Several aspects, including stability and turnover frequency, are addressed. In our study, the long-term electrooxidation of all three antibiotics was studied for 2 hours at 800 mV (*vs.* Ag/AgCl), and the data of the initial 6,000 s are shown for clarity. In all electrooxidation experiments, the concentration of $Cu(OH)_2$ catalyst is 0.1 mM, that is a typical concentration of Cu(II) species in wastewater [21].

Figure 7a shows the current-charge-time relation of ampicillin (0.1 and 1.0 mM) electrooxidation. Slight drop of pH from 13.07 to 13.04 is observed after electrolysis (1h), indicating the consumption of hydroxide species. With 0.1 mM ampicillin, the anodic current stabilizes at 6.9 μA after 2,000 s and maintains at 6.8 μA after 6,000 s. At higher ampicillin concentration of 1.0 mM, the current stabilizes at 9.6 μA after 1,000 s and stays at 9.4 μA at 6,000 s. Such performance shows the great stability of antibiotic electrooxidation in $Cu(OH)_2$ suspension. The corresponding UV-Vis spectra are shown in **Figure 7b**. The absorption band at 330 nm is assigned to the Cu(II)-ampicillin complex. At higher ampicillin concentrations, the equilibrium

(**Equation 2**) provides a nearly constant concentration of complex, while the substrate is consumed without the further formation of Cu(II)-ampicillin complex at lower ampicillin concentrations. The input charge is plotted against Cu(II)-ampicillin complex concentration in **Figure 7c**, in which a linear correlation with a slope value of -3.38 is found during the initial stage of electrooxidation (0~20 mC). The charge inputs higher than 20 mC cause less influence on the complex concentration, which can be explained with other competing reactions, such as further electrooxidation of products.

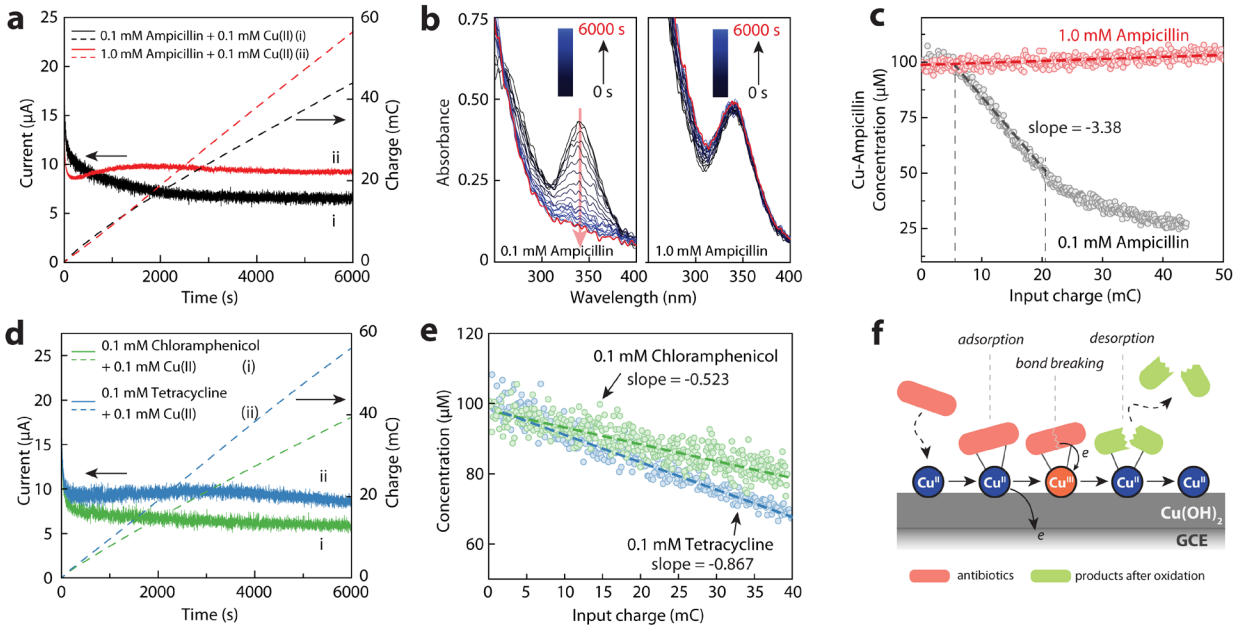

Figure 7. (a) Amperometric current-time (solid line) and charge-time (dotted line) curves in 0.1 M NaOH electrolyte with 0.1 mM $Cu(OH)_2$ containing 0.1 and 1.0 mM ampicillin; (b) Evolution of *in situ* UV-Vis absorbance spectra of electrolyte containing 0.1 and 1.0 mM ampicillin with 0.1 mM $Cu(OH)_2$ during electrooxidation; (c) Correlation of charge and Cu-ampicillin complex concentration with 0.1 and 1.0 mM ampicillin; (d) Amperometric current-time (solid line) and charge-time (dotted line) curves in 0.1 M NaOH electrolyte containing 0.1 mM tetracycline and 0.1 mM chloramphenicol with 0.1 mM $Cu(OH)_2$; (e) Correlation of charge and antibiotics concentration with antibiotics concentration of 0.1 mM; (f) Proposed reaction mechanism for electrooxidation of antibiotics with coexisting Cu species. The applied potential is 800 mV (*vs.* Ag/AgCl) and electrooxidation time is 6,000 s for amperometric studies.

For comparison, the electrooxidation of tetracycline and chloramphenicol are also studied with the same concentrations as in ampicillin studies. The current-charge-time plots and the correlation between the input charge and antibiotic concentration are shown in **Figures 7d** and **7e**, respectively. The high stability of the electrooxidation rate is also demonstrated for both antibiotics. Both electrooxidation experiments show an excellent linear relationship between input charge and concentration with a slope value of -0.867 (for tetracycline) and -0.523 (for chloramphenicol). Assuming a 100% faradic efficiency at the initial stage of electrooxidation, such slope values can be used to calculate the number of electrons transferred to oxidize one antibiotic molecule.

During a total period of τ, the charge Q is the electric current *i* integrated over time:

$$Q = \int_0^t i \, d\tau$$

where *t* is the total electrooxidation time.

According to Faraday's laws of electrolysis [45]:

$$Q = nF\Delta M = nF(C_0 - C_t)V$$

where *n* is the electron transfer number per molecule, *F* is the Faraday constant, ΔM is the mole difference of substance during electrooxidation time *t*, *V* is the electrolyte volume (2.50 mL), C_0 and C_t are the substance concentration at $\tau = 0$, and $\tau = t$.

Thus:

$$C_t = C_o - \frac{1}{nFV} Q$$

Therefore, the electron transfer number is 1.23 (~1) for ampicillin electrooxidation, 4.78 (~5) for tetracycline, and 7.93 (~8) for chloramphenicol.

Based on the previous analysis, the proposed general electrooxidation pathway is illustrated in **Figure 7f**. An equilibrium between surface Cu(II) species and antibiotics molecules is instantly

achieved in bulk solution. During the anodic potential sweep, depending on the type of antibiotic functional groups, electrons are transferred from antibiotics either *via* a Cu(III)-antibiotic intermediate or a direct route to form Cu(II)-oxidized antibiotics. Such complex further dissociates, releasing Cu(II) sites for the formation of the next Cu(II)-antibiotics complex.

3.7 Potential-dependent electrooxidation product analysis and reaction route

To resolve the mechanism of potential-dependent electrooxidation of antibiotics, the electrolyte before and after long-term electrooxidation was analyzed using UPLC-QTOF-MS. Two applied potentials (500 and 800 mV *vs.* SCE) are chosen to separate the stepwise electrooxidation processes and the corresponding products.

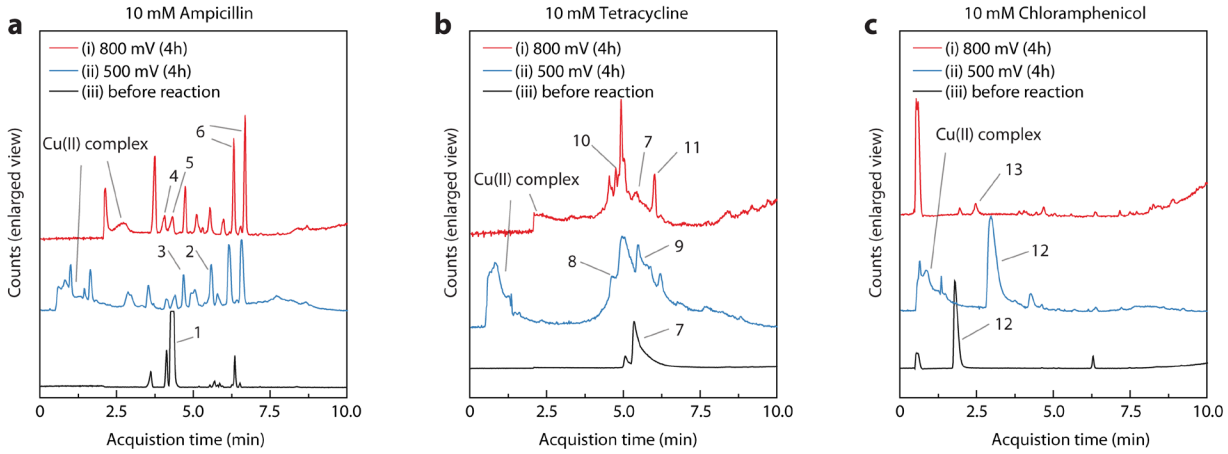

Figure 8. UPLC-QTOF-MS total ion chromatograms of (a) ampicillin, (b) tetracycline, and (c) chloramphenicol before and after the electrooxidation at 500 and 800 mV for 4h. The identified peaks are resolved.

The UPLC-QTOF-MS results are shown in **Figure 8**, and the corresponding structures are shown in **Figure 9** apart from the Cu(II) complex. The full analysis and identification of peaks can be found in the Supporting Information. Before the electrooxidation, the characteristic peaks for the antibiotic structures $[M+H]^+$ and their hydrolysis products (ampicillin and chloramphenicol)

are evident (structures **1**, **7**, and **12**). Upon the electrooxidation at 500 and 800 mV, various peaks corresponding to different products are suggested while only a trace amount of antibiotics remains. For ampicillin, as shown in **Figure 9a**, the active β-lactam group maintains at 400 mV but is found broken at 800 mV, which agrees with the results of using Cu(II) as a homogeneous catalyst.[28] Moreover, the existence of product **4** (*m/z* 122.06) and product **5** (*m/z* 164.08) demonstrates the further destruction of C-C bonding in the -NH_2-C-C=O unit, which is only observed by using high-valent Cu(III) catalysts, such as diperiodatocuprate(III) [46]. Such findings support our proposed catalytic reaction mechanism *via* Cu(III) formation. For tetracycline, **Figure 9b** suggests the stepwise oxidation of -OH functional groups, from structure **7** (*m/z* 445.16) to structures **8** (*m/z* 417.17) and **9** (*m/z* 399.16) at 500 mV, and eventually to structure **11** (*m/z* 187.04) at 800 mV. The full breakage of the backbone is suggested by product **11**, which is first reported herein. As to chloramphenicol, the treatment at 800 mV produces chemical **13** (*m/z* 138.06) while no observable electrooxidation products are evident at 500 mV. Once again, the C-C bond breaking in the HO-C-C-NH_2 structure is indicated, similar to homogeneous catalysis results [47]. Despite the existence of diverse products and interfering Cu(II) complex, it is convincing that the active structural fragments of antibiotics shown in **Figures 2a-2c** are all destroyed after the electrooxidation process at 800 mV. However, it should be noted that not all structures are resolved in our study due to the complicated structures involving complex and isomers.

3.8 The activity of antibiotics before and after electrooxidation

To confirm the deactivation of antibiotics after $Cu(OH)_2$-catalyzed electrooxidation, the activity of antibiotics is evaluated by minimum inhibitory concentration (MIC) values before and after a long-term electrooxidation treatment [22]. With an initial concentration of 0.5 mM, the electrooxidation was performed for 4 hours at 800 mV (*vs.* SCE) to allow full electrooxidation of

antibiotics. The pH of the electrolyte was tuned to 7.0 before activity evaluation. **Figure 10** shows the photo and illustration of the antibacterial activity test. From top to bottom, *E. coli* K-12 was treated with ampicillin, tetracycline, and chloramphenicol before and after electrooxidation. From left to right, the concentrations of antibiotics in each well were 50, 25, 12.5, 6.25, 3.13, 1.56, 0.78, 0.39, 0.20, 0.10, and 0 μM. The last column is medium only without bacterium. As illustrated, the MIC values of ampicillin, tetracycline, and chloramphenicol are 12.5, 1.56, and 12.5 μM, respectively. However, after the electrooxidation, the MIC values of all electrooxidation products are >50 μM. Such high values indicate the dramatic decrease of antibacterial activity after electrooxidation (at least a 4-fold decrease for ampicillin and chloramphenicol and a 32-fold decrease for tetracycline), which confirms the successful degradation of three antibiotics *via* electrooxidation method catalyzed by $Cu(OH)_2$.

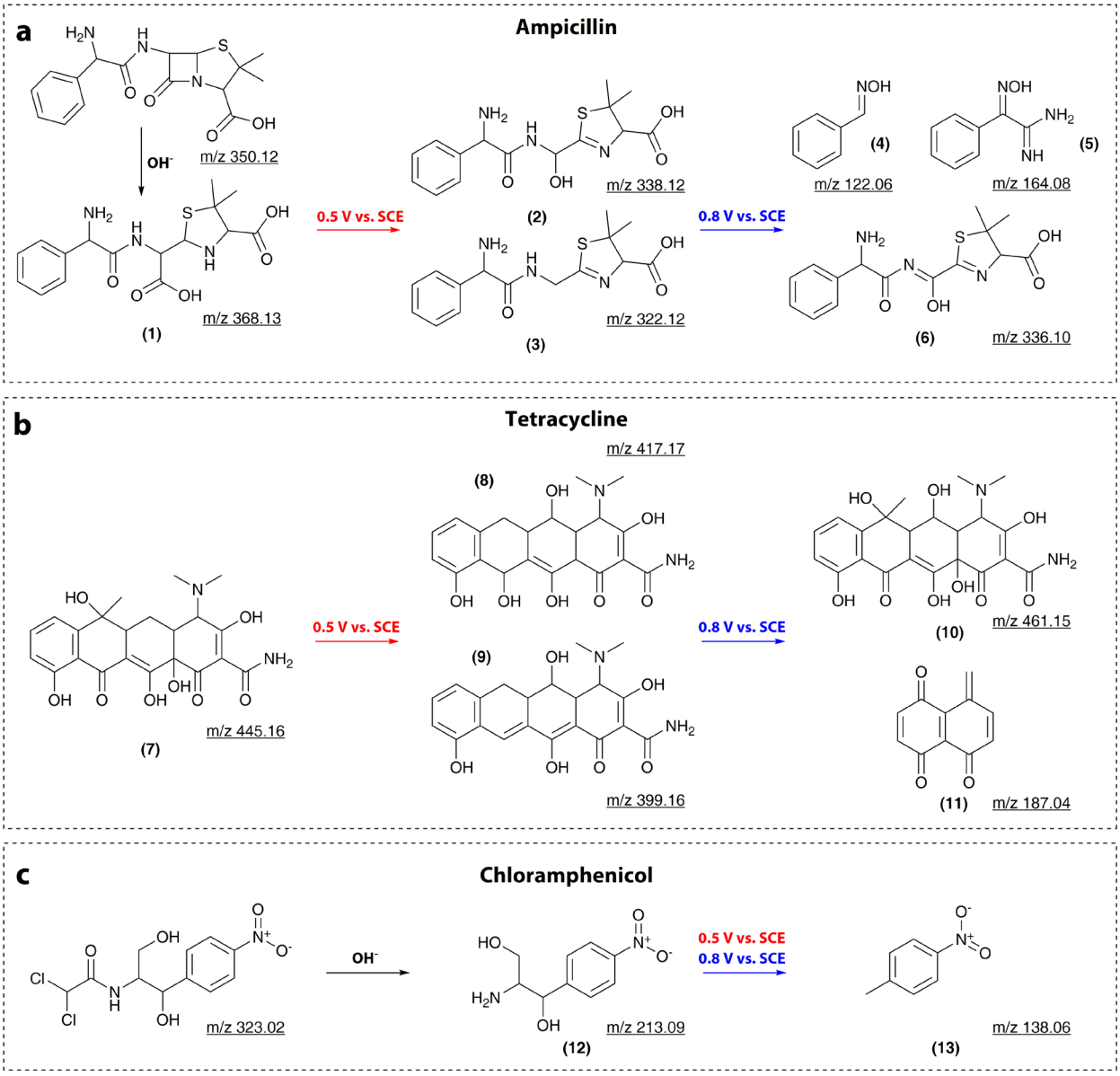

Figure 9. The proposed potential-dependent electrooxidation mechanism of antibiotics catalyzed by *in situ* formed $Cu(OH)_2$: (a) ampicillin; (b) tetracycline; (c) chloramphenicol. Insert *m/z* value indicates $[M+H]^+$.

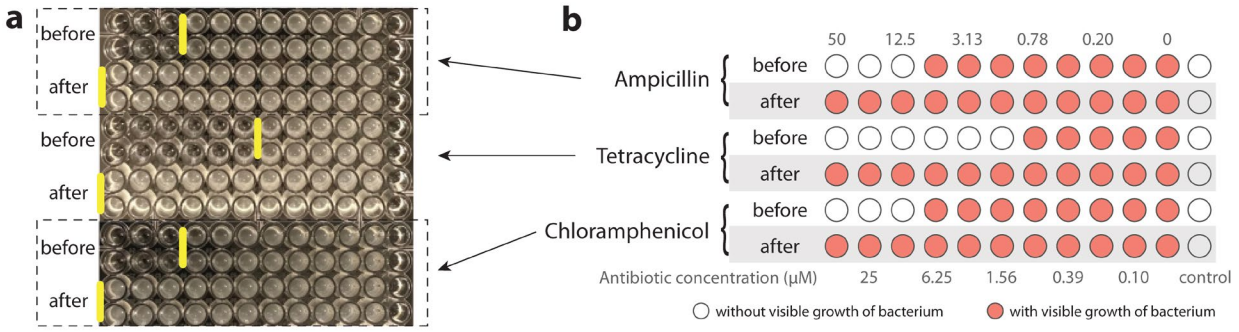

Figure 10. (a) Digital photo and (b) Illustration of antibacterial activity test by the microdilution method using ampicillin, tetracycline, and chloramphenicol before and after electrooxidation treatment.

3.9 Comparison between current electrochemical treatments

As previously stated, most of the current electrochemical treatments of antibiotics heavily relay on the production of hydroxyl radical (redox potential = 2.72 V *vs.* NHE), which is known as AOP, requiring O_2 supply. The comparison between different systems, especially when adopting different mechanisms such as the Cu(II)-catalyzed electrooxidation and the hydroxyl radical-mediated reaction, is highly challenging. On the one hand, many reports miss the data such as applied voltage, reporting regarding current density [48, 49]. While on the other hand, the degradation efficiency is evaluated using different aspects by researchers, such as the concentration ratio [48] and removal rate [50, 51], which also depend on the antibiotic concentration, applied voltage, reaction temperature, and electrode surface area. However, using the kinetic constant (assuming the first-order reaction for all, which, as shown in our voltammetry, is not correct) widely reported in different systems, we can roughly compare our results with current electrooxidation systems in **Table 2**.

Table 2. Comparison of the reported AOP and our Cu(II)-catalyzed antibiotics degredation.[1]

Antibiotics	Electrode Materials	Mechanism	Applied voltage	Kinetic constant (min^{-1}) × 10^{-3}	Ref.
Ampicillin	boron-doped diamond	AOP	unreported	~80	[48]
	$Cu(OH)_2$	catalytic	0.80 V (*vs.* SCE)	68.1	**This work**
Chloramphenicol	Al-doped PbO_2	AOP	unreported	9.8	[51]
	Cu	catalytic	0.30 V (cell voltage)	4.3	[52]
	$Cu(OH)_2$	catalytic	0.80 V (*vs.* SCE)	11.5	**This work**
Tetracycline	Ti/Ti_4O_7	AOP	~2.5 V (*vs.*SHE)	29	[53]
	Pb/PbO_2	AOP	unreported	61.2	[54]

	$Cu(OH)_2$	catalytic	0.80 V (*vs.* SCE)	35.4	**This work**

[1] The kinetic constants obtained under the closest conditions to ours are adopted from literature.

The kinetic constant obtained in our studies is similar, if not higher, to reported values. Considering that most of the reported values are evaluated using an advanced oxidation process (AOP) with very high potential (>2.72 V *vs*. NHE), our Cu(II)-catalyzed system is more energy-efficient and requires only 0.80 (*vs.* SCE), or 1.04 (*vs.* NHE).

4. Conclusion

In this study, the electrooxidation of antibiotics (ampicillin, chloramphenicol, and tetracycline) using *in situ* formed $Cu(OH)_2$ nanowires from coexisting Cu(II) species as an electrocatalyst in the alkaline electrolyte was studied for the first time. Highly efficient electrooxidation of all three antibiotics is demonstrated. Based on both dc voltammetry and FTacV results, a stepwise electrochemical processes are evident for the electrooxidation of ampicillin and tetracycline, while one process is suggested for chloramphenicol. The kinetic studies show two kinetic regions for ampicillin (300 ~ 500 mV and 500 ~ 800 mV, *vs.* SCE) and tetracycline (350 ~ 450 mV and 450 ~ 800 mV, *vs.* SCE), whereas only one kinetic region is suggested for chloramphenicol within the studied potential range (300 ~ 800 mV, *vs.* SCE). The oxidation of Cu(II) to Cu(III) at ~520 mV (*vs.* SCE) is essential for antibiotics electrooxidation, as suggested by FTacV. Using $Cu(OH)_2$ as an electrochemical sensor at 600 mV (*vs.* SCE), a high sensitivity values are obtained (45.1 mA mM^{-1} cm^{-2} for ampicillin; 271.6 mA mM^{-1} cm^{-2} for chloramphenicol; and 443.5 mA mM^{-1} cm^{-2} for tetracycline).

Studies using *in situ* UV-vis spectroelectrochemistry indicate that the soluble $Cu(OH)_y^{x-}$ on the surface of $Cu(OH)_2$ nanowires, other than CuO, acts as active site during the electrooxidation process, which can be regenerated upon the formation and dissociation of Cu(II)-antibiotic

complex. Moreover, both direct electrooxidation of antibiotics and electrooxidation *via* Cu(III)-antibiotics intermediate are involved. Long-term electrooxidation shows the high stability and efficiency of electrochemical removal of antibiotics, and electron transfer numbers are estimated to be 1.23 (~1) for ampicillin electrooxidation, 4.78 (~5) for tetracycline, and 7.93 (~8) for chloramphenicol at 800 mV (*vs.* Ag/AgCl). UPLC-QTOF-MS results indicate that the active structural fragments of antibiotics responsible for targeting bacteria are destroyed after the electrooxidation treatment at 800 mV (*vs.* SCE). Further activity test of antibiotics using *E. coli* confirms the deactivation after electrooxidation treatment.

Compared with the established AOP methods for antibiotics degradation, the Cu(II)-catalyzed electrooxidation exhibits similar reaction rates at a much lower applied potential, showing higher energy efficiency. This work demonstrates that the Cu(II)-based electrocatalytic system can offer a cheap and efficient approach towards antibiotics sensing and removal from wastewater.

Acknowledgements

This work was supported by the Innovation and Technology Commission of Hong Kong and the Hong Kong Polytechnic University (Grant No. G-YBSZ and 1-BE0Y). We also acknowledged the technical support from the University Facility in Life Science (ULS) of the Hong Kong Polytechnic University.

Supporting Information

The calculation details, staircase cyclic voltammograms, and detailed UPLC-QTOF-MS results are available in supporting information.

Conflict of Interest

The authors declare no conflict of interest.

ORCID

Dr. Weiran Zheng 0000-0002-9915-6982

Dr. Yun-Chung Leung 0000-0003-3590-7027

Dr. Lawrence Yoon Suk Lee 0000-0002-6119-4780

Author contribution

Dr. W. Zheng conducted the electrochemical experiments (CV, *i*-t test, and *in-situ* spectroelectrochemistry) and the XRD characterization and analysis. Dr. C.-S. Tsang carried out the UPLC-QTOF-MS analysis. Dr. L. Y. So tested the antibiotics activity. M. Liu carried out TEM characterization. Dr. Y.-C. Leung designed the antibiotics activity test and Dr. L. Y. S. Lee supervised the progress of this project and drafted the manuscript with Dr. W. Zheng.

References

[1] P. Verlicchi, M. Al Aukidy, E. Zambello, Sci. Total Environ., 429 (2012) 123-155.
[2] Y. Luo, L. Xu, M. Rysz, Y. Wang, H. Zhang, P.J. Alvarez, Environ Sci Technol, 45 (2011) 1827-1833.
[3] Q.Q. Zhang, G.G. Ying, C.G. Pan, Y.S. Liu, J.L. Zhao, Environ Sci Technol, 49 (2015) 6772-6782.
[4] B. Wang, X.L. Lv, D. Feng, L.H. Xie, J. Zhang, M. Li, Y. Xie, J.R. Li, H.C. Zhou, J Am Chem Soc, 138 (2016) 6204-6216.
[5] L. Kovalova, H. Siegrist, H. Singer, A. Wittmer, C.S. McArdell, Environ Sci Technol, 46 (2012) 1536-1545.
[6] B. Tiwari, B. Sellamuthu, Y. Ouarda, P. Drogui, R.D. Tyagi, G. Buelna, Bioresour. Technol., 224 (2017) 1-12.
[7] X. Luo, Z. Zheng, J. Greaves, W.J. Cooper, W. Song, Water Res., 46 (2012) 1327-1336.
[8] L. Jiang, X. Yuan, G. Zeng, Z. Wu, J. Liang, X. Chen, L. Leng, H. Wang, H. Wang, Appl. Catal., B, 221 (2018) 715-725.
[9] Infectious Diseases, Elsevier2017.
[10] E. Brillas, I. Sires, M.A. Oturan, Chem. Rev., 109 (2009) 6570-6631.
[11] N. Barhoumi, H. Olvera-Vargas, N. Oturan, D. Huguenot, A. Gadri, S. Ammar, E. Brillas, M.A. Oturan, Appl. Catal., B, 209 (2017) 637-647.
[12] R. Kaur, J.P. Kushwaha, N. Singh, Chemosphere, 193 (2018) 685-694.
[13] D. Shan, S. Deng, C. Jiang, Y. Chen, B. Wang, Y. Wang, J. Huang, G. Yu, M.R. Wiesner, Environ. Sci.: Nano, 5 (2018) 1650-1660.
[14] W. Wang, J. Yu, J. Zou, X. Yu, Electrochim. Acta, 191 (2016) 426-434.
[15] S.D. Jojoa-Sierra, J. Silva-Agredo, E. Herrera-Calderon, R.A. Torres-Palma, Sci. Total Environ., 575 (2017) 1228-1238.
[16] C.C. Jara, D. Fino, V. Specchia, G. Saracco, R. Spinelli, Appl. Catal., B, 70 (2007) 479-487.
[17] S. Liu, Y. Wang, X. Zhou, W. Han, J. Li, X. Sun, J. Shen, L. Wang, Electrochim. Acta, 253 (2017) 357-367.
[18] W. Zheng, Y. Li, L.Y.S. Lee, Electrochim. Acta, 308 (2019) 9-19.
[19] Z. Wu, Z. Zhang, L. Liu, Electrochim. Acta, 42 (1997) 2719-2723.
[20] W. Zheng, Y. Li, M. Liu, C.-S. Tsang, L.Y.S. Lee, K.-Y. Wong, Electroanalysis, 30 (2018) 1446-1454.
[21] W. Ben, Z. Qiang, C. Adams, H. Zhang, L. Chen, J. Chromatogr. A, 1202 (2008) 173-180.
[22] I. Wiegand, K. Hilpert, R.E. Hancock, Nat Protoc, 3 (2008) 163-175.
[23] L. Hidmi, M. Edwards, Environ. Sci. Technol., 33 (1999) 2607-2610.
[24] G.H. Du, G. Van Tendeloo, Chem. Phys. Lett., 393 (2004) 64-69.
[25] L. Wang, K. Zhang, Z. Hu, W. Duan, F. Cheng, J. Chen, Nano Res., 7 (2013) 199-208.
[26] H.R. Oswald, A. Reller, H.W. Schmalle, E. Dubler, Acta Crystallogr., Sect. C: Cryst. Struct. Commun., 46 (1990) 2279-2284.
[27] M.G.A. El-Wahed, M.S. Refat, S.M. El-Megharbel, J. Mol. Struct., 892 (2008) 402-413.
[28] Y. Guo, D.C.W. Tsang, X. Zhang, X. Yang, Environ. Sci. Pollut. Res., 25 (2018) 4279-4288.
[29] B. Carlotti, A. Cesaretti, F. Elisei, Phys. Chem. Chem. Phys., 14 (2012) 823-834.

[30] Y.-H. Wang, J.-B. He, Electrochim. Acta, 66 (2012) 45-51.
[31] A. El-Trass, H. ElShamy, I. El-Mehasseb, M. El-Kemary, Appl. Surf. Sci., 258 (2012) 2997-3001.
[32] A. Sher, M. Veber, M. Marolt-Gomiscek, S. Gomiscek, Int. J. Pharm., 90 (1993) 181-186.
[33] Y. Zhao, Y. Tan, Y. Guo, X. Gu, X. Wang, Y. Zhang, Environ. Pollut., 180 (2013) 206-213.
[34] W. Zheng, Y. Li, C.-S. Tsang, L. Hu, M. Liu, B. Huang, L.Y.S. Lee, K.-Y. Wong, ChemElectroChem, 4 (2017) 2788-2792.
[35] S.X. Guo, Y. Liu, A.M. Bond, J. Zhang, P. Esakki Karthik, I. Maheshwaran, S. Senthil Kumar, K.L. Phani, Phys. Chem. Chem. Phys., 16 (2014) 19035-19045.
[36] Z.G. Yu, R.Y. Lai, Talanta, 176 (2018) 619-624.
[37] A. Munawar, M.A. Tahir, A. Shaheen, P.A. Lieberzeit, W.S. Khan, S.Z. Bajwa, J. Hazard. Mater., 342 (2018) 96-106.
[38] R. Karthik, M. Govindasamy, S.M. Chen, V. Mani, B.S. Lou, R. Devasenathipathy, Y.S. Hou, A. Elangovan, J. Colloid Interface Sci., 475 (2016) 46-56.
[39] S.M. Taghdisi, N.M. Danesh, M. Ramezani, K. Abnous, Biosens. Bioelectron., 85 (2016) 509-514.
[40] R.T. Kushikawa, M.R. Silva, A.C.D. Angelo, M.F.S. Teixeira, Sens. Actuators, B, 228 (2016) 207-213.
[41] R. Guidelli, R.G. Compton, J.M. Feliu, E. Gileadi, J. Lipkowski, W. Schmickler, S. Trasatti, Pure Appl. Chem., 86 (2014) 245-258.
[42] J. Wu, X. Li, B. Yadian, H. Liu, S. Chun, B. Zhang, K. Zhou, C.L. Gan, Y. Huang, Electrochem. Commun., 26 (2013) 21-24.
[43] N.R. Dhineshbabu, V. Rajendran, N. Nithyavathy, R. Vetumperumal, Appl. Nanosci., 6 (2015) 933-939.
[44] W. Zheng, Y. Li, L. Hu, L.Y.S. Lee, Sens. Actuators, B, 282 (2019) 187-196.
[45] A.J. Bard, L.R. Faulkner, Electrochemical Methods: Fundamentals and Applications, 2nd ed., Wiley, 2000.
[46] N.P. Shetti, R.N. Hegde, S.T. Nandibewoor, J. Mol. Struct., 930 (2009) 180-186.
[47] K. Byadagi, M. Meti, S. Nandibewoor, S. Chimatadar, Ind. Eng. Chem. Res., 52 (2013) 9011-9020.
[48] Z. Frontistis, D. Mantzavinos, S. Meric, J. Environ. Manage., 223 (2018) 878-887.
[49] N. Oturan, J. Wu, H. Zhang, V.K. Sharma, M.A. Oturan, Appl. Catal., B, 140 (2013) 92-97.
[50] R. Karthik, J.V. Kumar, S.M. Chen, C. Karuppiah, Y.H. Cheng, V. Muthuraj, ACS Appl. Mater. Interfaces, 9 (2017) 6547-6559.
[51] J.M. Chen, Y.J. Xia, Q.Z. Dai, Electrochim. Acta, 165 (2015) 277-287.
[52] D. Wu, F. Sun, Y. Zhou, Electrochim. Acta, 240 (2017) 136-145.
[53] J.B. Wang, D. Zhi, H. Zhou, X.W. He, D.Y. Zhang, Water Res., 137 (2018) 324-334.
[54] I. Yahiaoui, F. Aissani-Benissad, F. Fourcade, A. Amrane, Chem. Eng. J., 221 (2013) 418-425.

Table of Content